A toolbox of Cre-dependent optogenetic transgenic mice for light-induced activation and silencing

Linda Madisen[1], Tianyi Mao[2,7], Henner Koch[3], Jia-min Zhuo[4], Antal Berenyi[5], Shigeyoshi Fujisawa[5], Yun-Wei A. Hsu[3], Alfredo J. Garcia III[3], Xuan Gu[4], Sebastien Zanella[3], Jolene Kidney[1], Hong Gu[1], Yimei Mao[4], Bryan M. Hooks[2], Edward S. Boyden[6], György Buzsáki[5], Jan Marino Ramirez[3], Allan R. Jones[1], Karel Svoboda[2], Xue Han[4], Eric E. Turner[3], Hongkui Zeng[1]*

Supplementary Information

Supplementary Figure 1. Baseline fluorescence level in the reporter lines in the absence of Cre, as well as Cre-induced transgene expression in *Pvalb*-IRES-Cre. (**a**) No baseline fluorescence above background in Ai27, Ai32, Ai35 and Ai39 reporter mice alone (without Cre induction). Areas shown: first row, cortex; second row, hippocampus; third row, striatum and thalamus. Scale bar, 200 μm. Bottom row shows confocal images of the CA1 pyramidal neurons. Scale bar, 20 μm. (**b**) Confocal images in the cortex showing Cre-induced transgene expression at native fluorescence level in *Pvalb*+ neurons in *Pvalb*-IRES-Cre;Ai27, *Pvalb*-IRES-Cre;Ai32, *Pvalb*-IRES-Cre;Ai35, *Pvalb*-IRES-Cre;Ai39 mice. White arrowheads point to ring-shaped cell bodies with no intracellular aggregates, indicating protein localization to the cell membrane and processes. Scale bar, 20 μm. Both ChR2-EYFP in Ai32 and Arch-EGFP-ER2 in Ai35 exhibit strong fluorescence, indicating they have high-level protein expression. Strong fluorescence for ChR2-tdTomato in Ai27 was also observed, however, because of the fast bleaching of tdTomato under confocal microscope, the ChR2-tdTomato fluorescence does not appear to be prominent in the image shown. On the other hand, eNpHR3.0-EYFP in Ai39 exhibits significantly weaker fluorescence, indicating lower-level protein expression.

Supplementary Figure 1

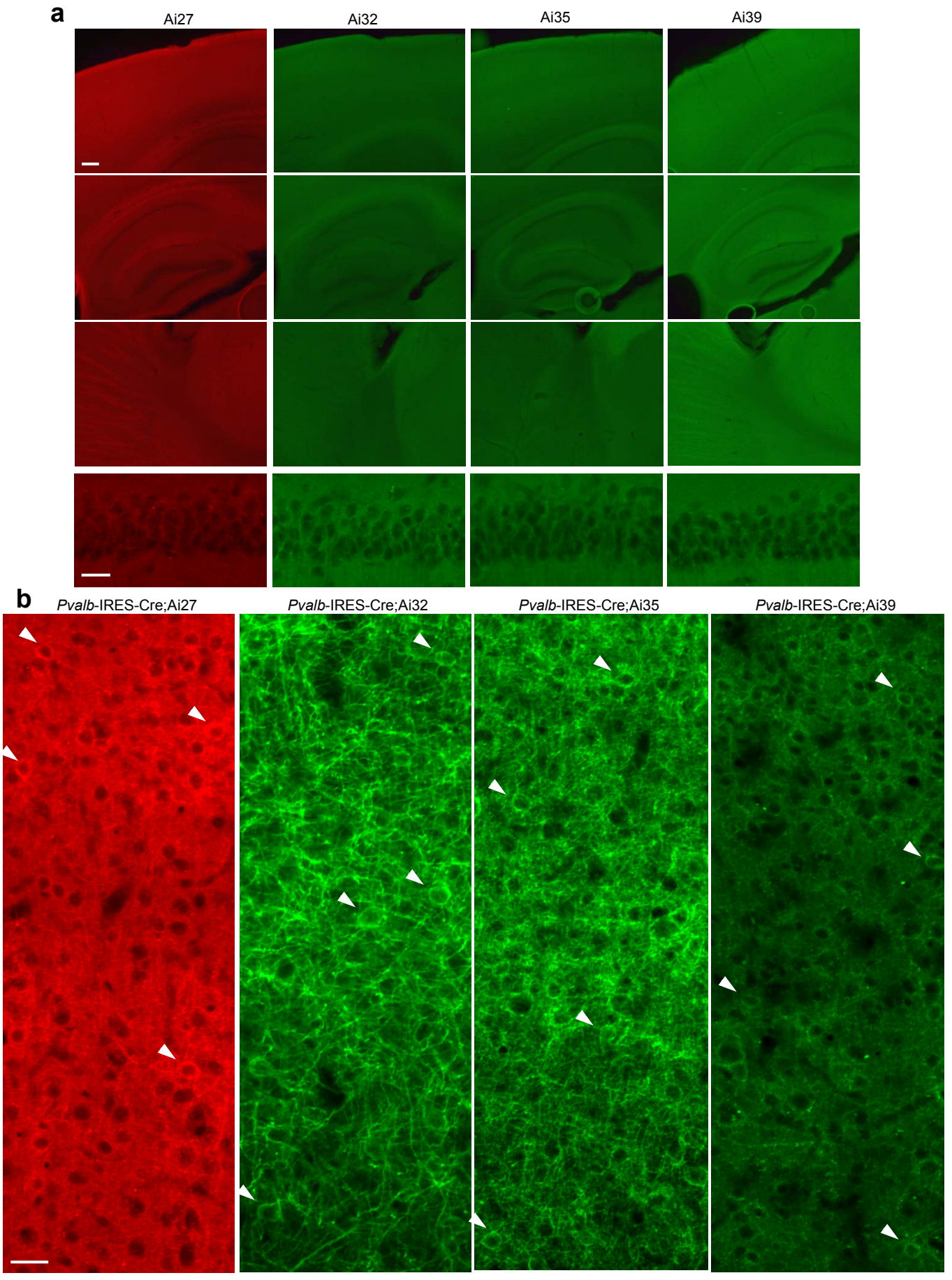

Supplementary Figure 2

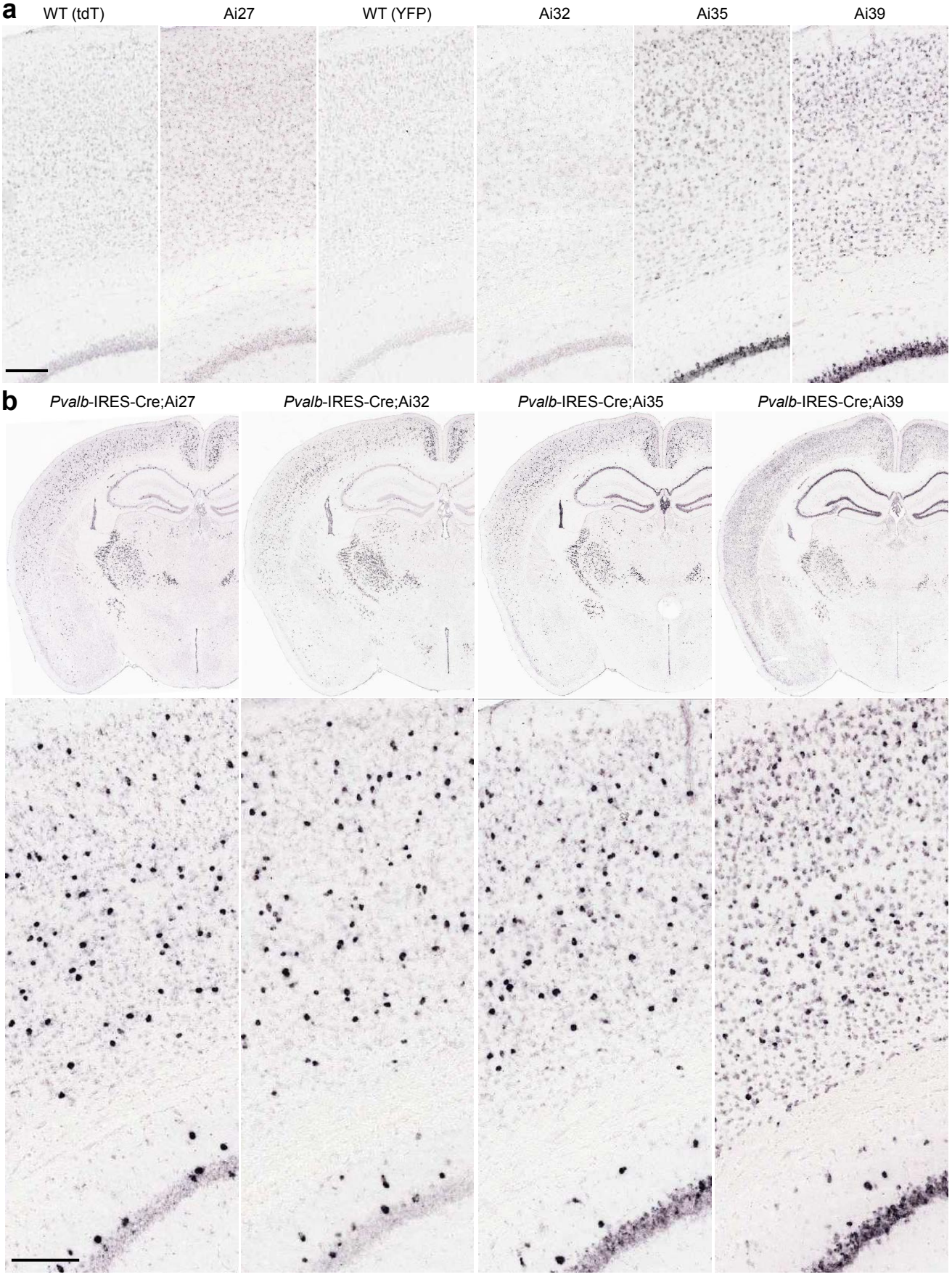

Supplementary Figure 2. Additional ISH expression data showing baseline mRNA levels in the reporter lines in the absence of Cre, as well as Cre-induced mRNA levels in reporters crossed to *Pvalb*-IRES-Cre. (**a**) Baseline mRNA levels in cortex and hippocampus in Ai27, Ai32, Ai35 and Ai39 reporter mice alone (without Cre induction). Wildtype (WT) mouse sections were used as negative controls for the tdTomato (tdT) probe used in Ai27 and the EYFP probe used in Ai32, Ai35 and Ai39. Leaky expression in these areas at the mRNA level was observed in Ai35 mice at low level (mainly in hippocampus), and in Ai39 mice at significant level (mainly in cortex and hippocampus) (also observable in **b**). Although the cause of this unexpected leakage in only certain lines is unknown, as the sequences of the targeting vectors were identical except for the transgenes themselves and their neighboring restriction sites for cloning, one possibility might be that there is cryptic transcriptional start or splicing acceptor site(s) in the transgene sequence that could lead to low-level skipping of the stop cassette in front of the transgene. (**b**) Strong Cre-induced transgene expression at mRNA levels in *Pvalb*+ neurons in *Pvalb*-IRES-Cre;Ai27, *Pvalb*-IRES-Cre;Ai32, *Pvalb*-IRES-Cre;Ai35, *Pvalb*-IRES-Cre;Ai39 mice (ages P148-151). Note the substantially higher signals in targeted cells above the baseline background in each mouse line. Scale bars, 200 μm.

Supplementary Figure 3. Additional ISH expression data showing strong Cre-induced transgene expression throughout the brain. The ages of all mice used were ~P56. (**a**) ChR2-tdTomato mRNA expression in cholinergic neurons in the basal forebrain (middle panel) and brainstem (bottom panel) in *Chat*-IRES-Cre;Ai27 mice. (**b**) ChR2-EYFP mRNA expression in cholinergic neurons in the basal forebrain (middle panel) and brainstem (bottom panel) in *Chat*-IRES-Cre;Ai32 mice. (**c**) Arch-EGFP-ER2 mRNA expression in widespread brain regions, including cortex (middle panel), striatum and thalamus (both shown in bottom panel) in *Camk2a*-CreERT2;Ai35 mice after tamoxifen induction. (**d**) eNpHR3.0-EYFP mRNA expression in widespread brain regions, including cortex (middle panel), striatum and thalamus (both shown in bottom panel) in *Camk2a*-CreERT2;Ai39 mice after tamoxifen induction. Scale bar, 200 μm.

Supplementary Figure 3

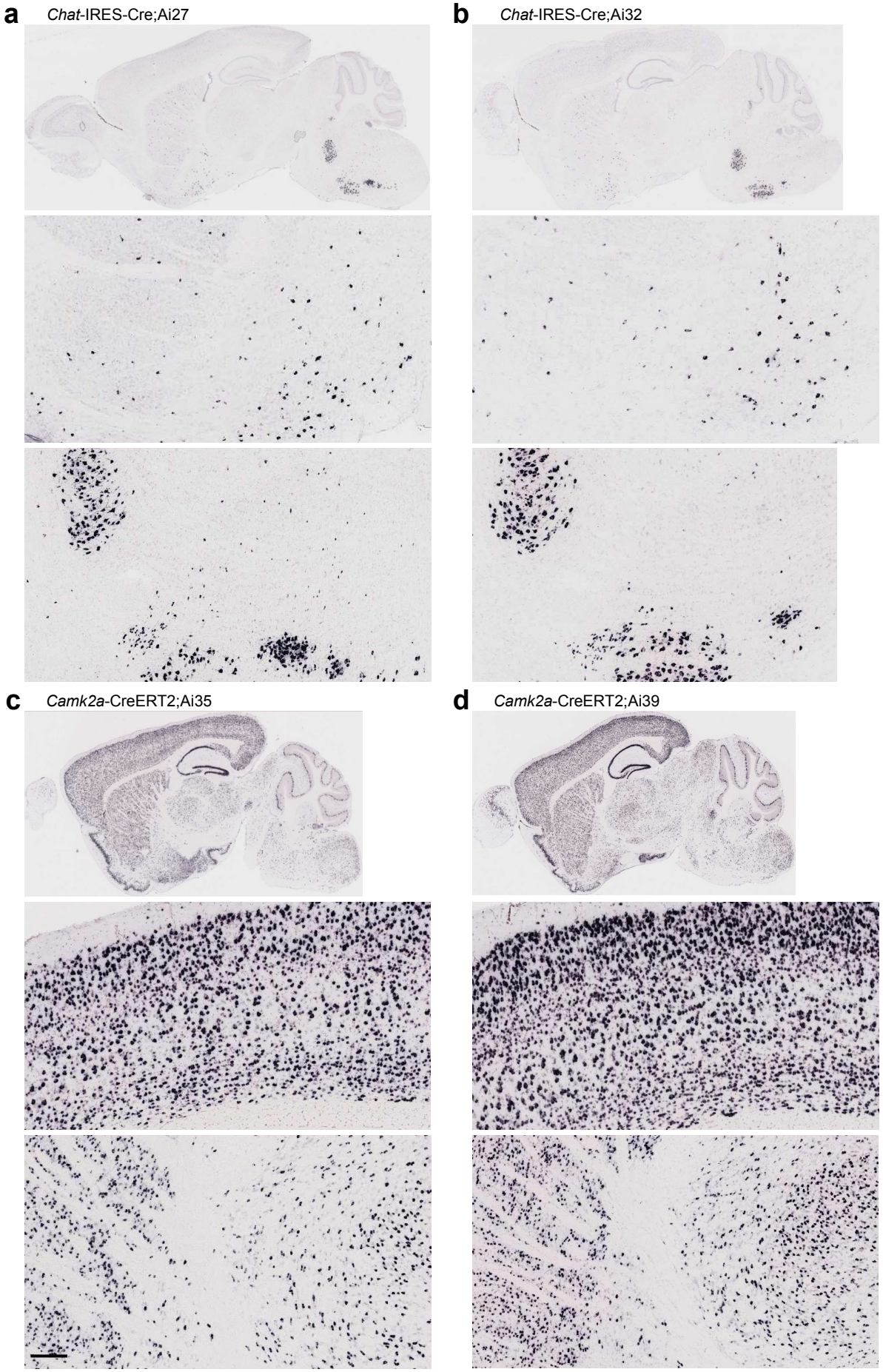

Supplementary Figure 4

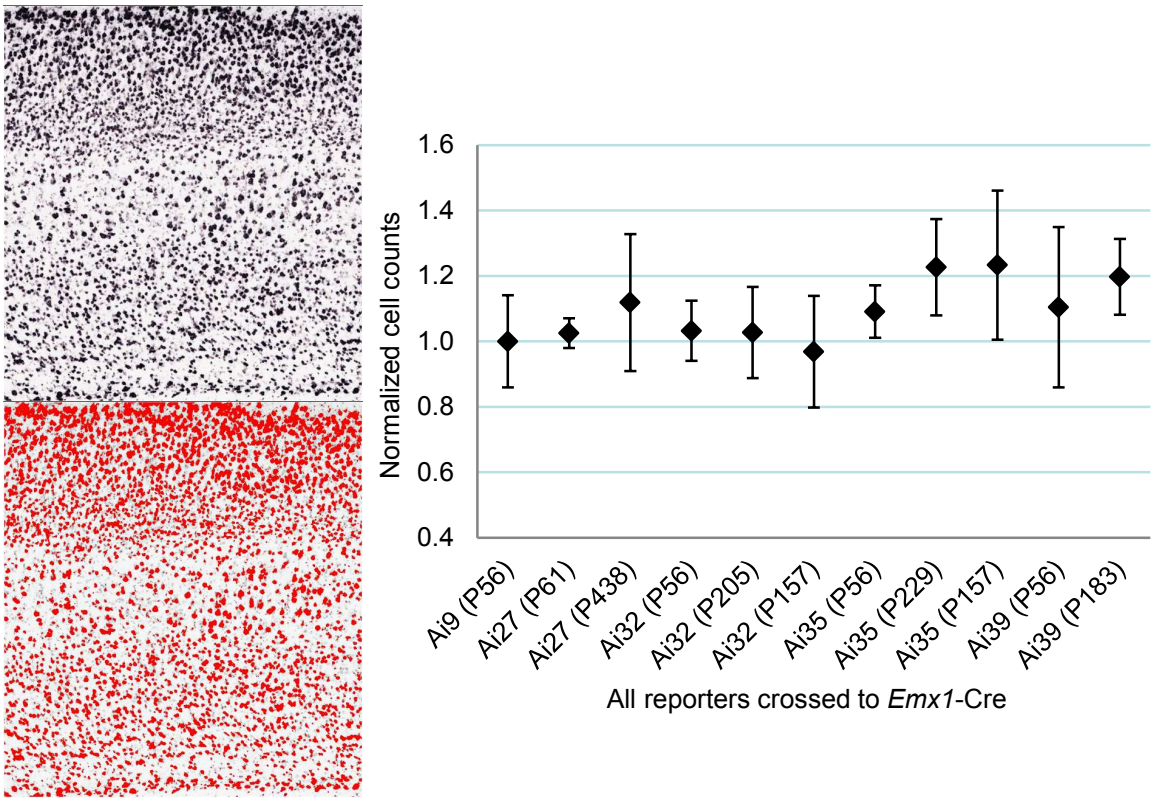

Supplementary Figure 4. Quantification of the number of Cre-induced reporter-expressing cells from reporter ISH images in the cortex of *Emx1*-Cre;Ai27, *Emx1*-Cre;Ai32, *Emx1*-Cre;Ai35 and *Emx1*-Cre;Ai39 mice of various ages. Each data point represents the average cell count from one mouse. For each line, one younger mouse (P56 or P61) and 1-2 older mice (P157-P438, oldest available ones in our mouse colony at the time of experiment) were used for the cell counting. A P56 *Emx1*-Cre;Ai9 mouse was used as control (Ai9: the tdTomato-expressing Cre reporter [9]). Although not fully shown here, the reporter ISH pattern of every mouse used appeared identical to that shown in **Figure 1d**. For counting of transgene-expressing cells, 3 ROIs (regions of interest) spanning the entire cortical depth were chosen, one each from motor, somatosensory or visual cortical area. The number of expressing cells in each ROI was estimated using the Analyze Particles application in the Fiji image analysis software. One example ROI (from the oldest mouse, P438 *Emx1*-Cre;Ai27) is shown here. Upper panel is the raw ISH image, and lower panel is the image after thresholding with particles to be counted highlighted in red. Normalized cell counts (Y-axis) refer to the average cell count per unit area for each mouse normalized to that of the *Emx1*-Cre;Ai9 control mouse which was set to 1. Each data point is mean ± s.d. There is no significant difference between *Emx1*-Cre;Ai9 and any of the other mouse ($p > 0.1$, unpaired student's t-test). The normal ISH expression pattern and normal cell counts for all these mice indicate that long-term expression of all the optogenetic molecules at levels attained in these transgenic lines did not have toxicity.

Supplementary Figure 5

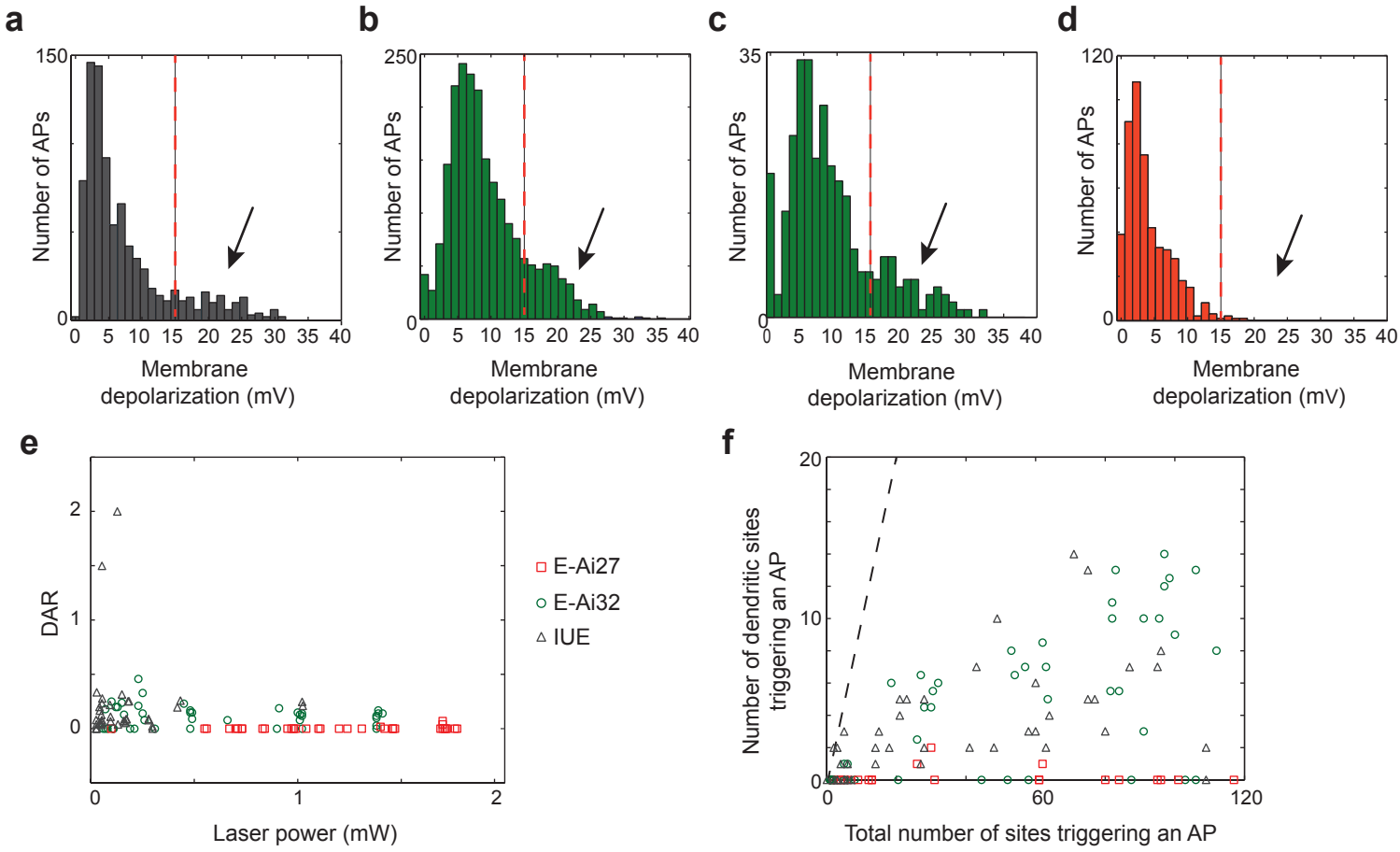

Supplementary Figure 5. Preferential photoexcitability in dendrites or axons of *Emx1*-Cre;Ai27 (abbreviated as E-Ai27) and *Emx1*-Cre;Ai32 (abbreviated as E-Ai32) mice. (**a-d**) Histograms of membrane potentials at the inflection points (also see Methods) for (**a**) *in utero* electroporated (IUE) cells (n = 6), (**b**) E-Ai32 cells (n = 9), (**c**) E-Ai32 cells around threshold laser power (n = 9, laser power 30-200 μW), and (**d**) E-Ai27 cells (n = 12). For each cell, responses from all laser power stimulations are included. Red dashed lines indicate the threshold (15 mV) for determining axonal versus somatic/dendritic responses. Somatic/dendritic components are indicated by arrows. In both ChR2-Venus IUE cells (**a**) and E-Ai32 cells (**b, c**), more AP events had pre-spiking membrane potentials greater than the 15-mV threshold, indicating a somatic/dendritic component that was nearly absent in E-Ai27 cells (**d**). (**e**) The ratio of the number of the photostimulation sites triggering action potentials in somata and dendrites to the number of sites triggering action potentials in axons (DAR) plotted against the laser power used for photostimulation. Green circles: E-Ai32 cells; red squares: E-Ai27 cells; gray triangles: ChR2-Venus IUE cells. Each point represents DAR calculated from one trial in the corresponding animal group. (**f**) The number of the photostimulation sites triggering action potentials in somata and dendrites plotted against the total number of photostimulation sites triggering action potentials. The black dotted line (slope of 1) indicates the positions when all stimulation sites are somatic/dendritic.

Supplementary Figure 6

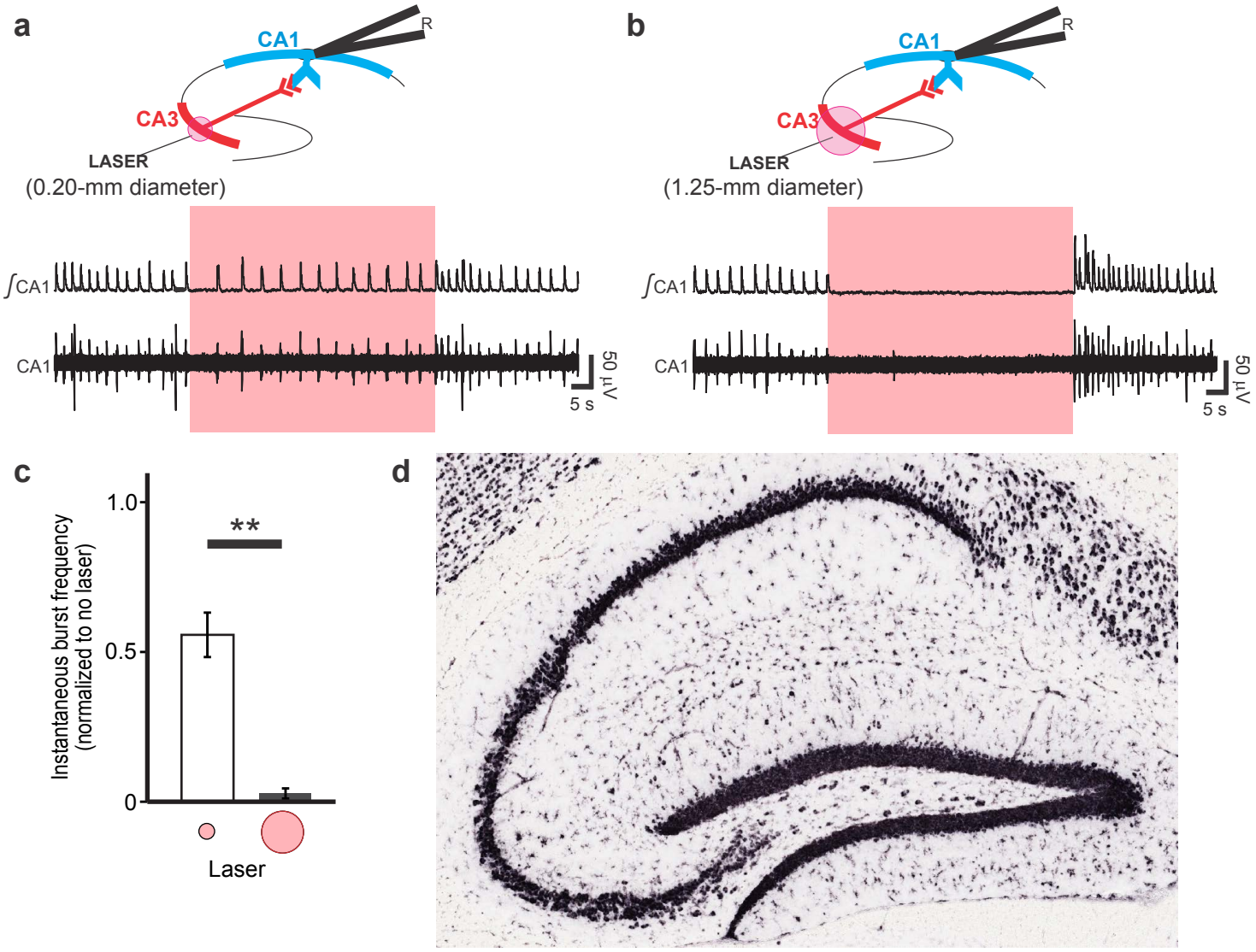

Supplementary Figure 6. Inhibition of the hippocampal network in *Emx1*-Cre;Ai35 mice is dependent on the area of illumination of CA3. The experimental design was similar to that in **Figure 5**, in which activity in CA1 was inhibited by optogenetic silencing of CA3. However, in this experiment, a laser (640 nm) was used instead of an LED to give more precise control over the area of illumination, and the total light power was varied to maintain constant illumination per unit area (35 mW mm^{-2}) while the area was varied by changing the distance from the end of the optical fiber to the surface of the slice. Adult mice approximately 6 months of age were used. (**a**) Illumination of a 0.20-mm diameter area of CA3 reversibly attenuated, but did not completely inhibit, postsynaptic bursting of area CA1 neurons. (**b**) Increasing the diameter of the area of illumination to 1.25 mm of CA3 resulted in nearly complete inhibition of the postsynaptic bursting of area CA1 neurons, but still allowed reversal, with some rebound increase in activity noted. (**c**) Summary of the degree of laser-mediated inhibition of postsynaptic CA1 neuronal bursting based on the instantaneous frequency of population bursting normalized to the period prior to laser exposure, for three separate trials. Smaller circle (left) represents a light zone with a 0.20-mm diameter (n = 3). Larger circle (right) represents a light zone with a 1.25-mm diameter (n = 3). Increasing the diameter of the light zone significantly increases the degree of inhibition in area CA1 (** $p < 0.01$, paired student's t-test). Data expressed as mean ± s.d. (**d**) Reporter transgene expression by ISH in the hippocampus of *Emx1*-Cre;Ai35 mouse, showing near 100% expression in the excitatory neurons in the CA1, CA3 and dentate gyrus subfields.

Supplementary Figure 7

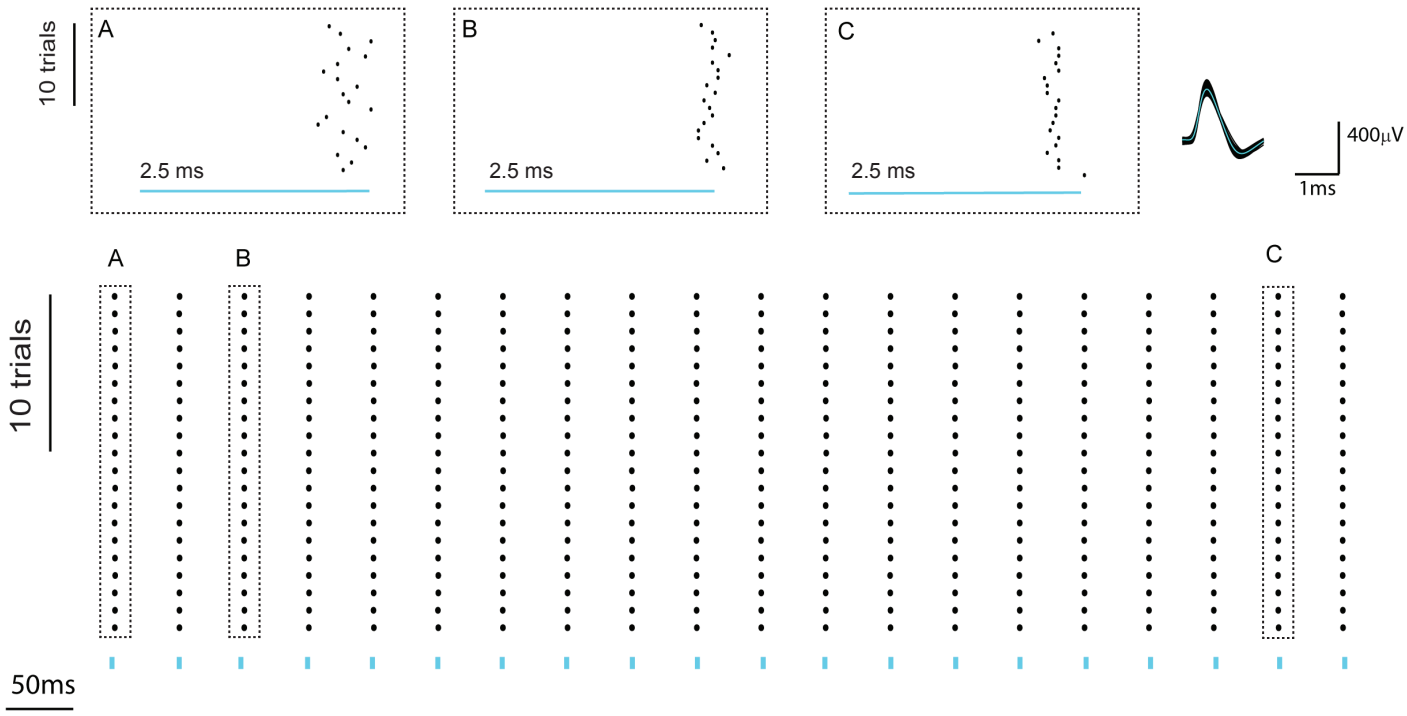

Supplementary Figure 7. Light evoked spiking in *Emx1*-Cre;Ai32 mouse with the sub-millisecond temporal precision. Spike raster plot and waveforms in a representative neuron upon blue light illumination (20-Hz pulse trains with 2.5-ms pulses, ~3 mW mm^{-2} at the optical fiber tip which is ~500 μm above recording electrode). The upper inserts A, B and C demonstrate the timing of each spike upon illumination by the 1st, 3rd, and 19th pulse of the light pulse train, across 20 repetitions.

Supplementary Figure 8

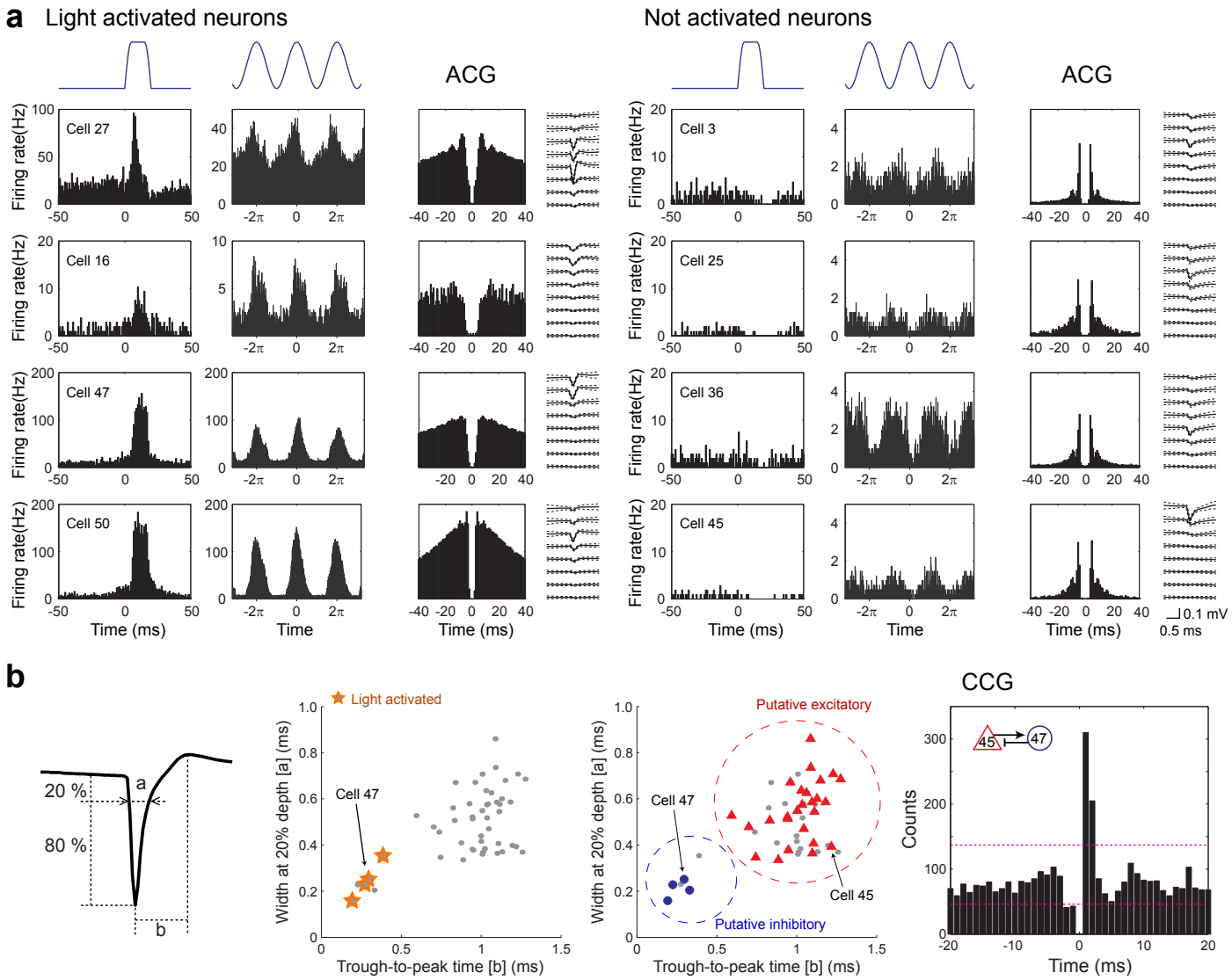

Supplementary Figure 8. Excitation of ChR2-expressing neurons in the hippocampal CA1 of *Pvalb*-IRES-Cre;Ai32 mice during waking state. (**a**) PSTHs of example neurons (additional to **Fig. 7a**), which were transiently activated (left 4 neurons) and transiently suppressed (right 4 neurons) by a single light pulse and sinus (8 Hz) stimulation. Autocorrelogram (ACG) and waveform of each neuron are also shown. Light intensity was 1 mW. (**b**) Physiological and optogenetic classification of neuron types in the hippocampus. Left panel, spike width and trough-to-peak time of the wide-band (1 Hz - 5 kHz) waveform of pyramidal neuron spikes. Middle panels, segregation of simultaneously recorded neurons by these two parameters. Middle left, light-activated neurons are marked with orange stars. Middle right, putative pyramidal cells and interneurons are indicated in the same plot as middle left. Red triangles and blue circles (Middle panels) indicate excitatory and inhibitory neurons identified by monosynaptic interactions, calculated from their cross-correlogram (Right panel). Note strong overlap between the physiologically characterized groups and the optogenetically characterized groups.

Supplementary Figure 9

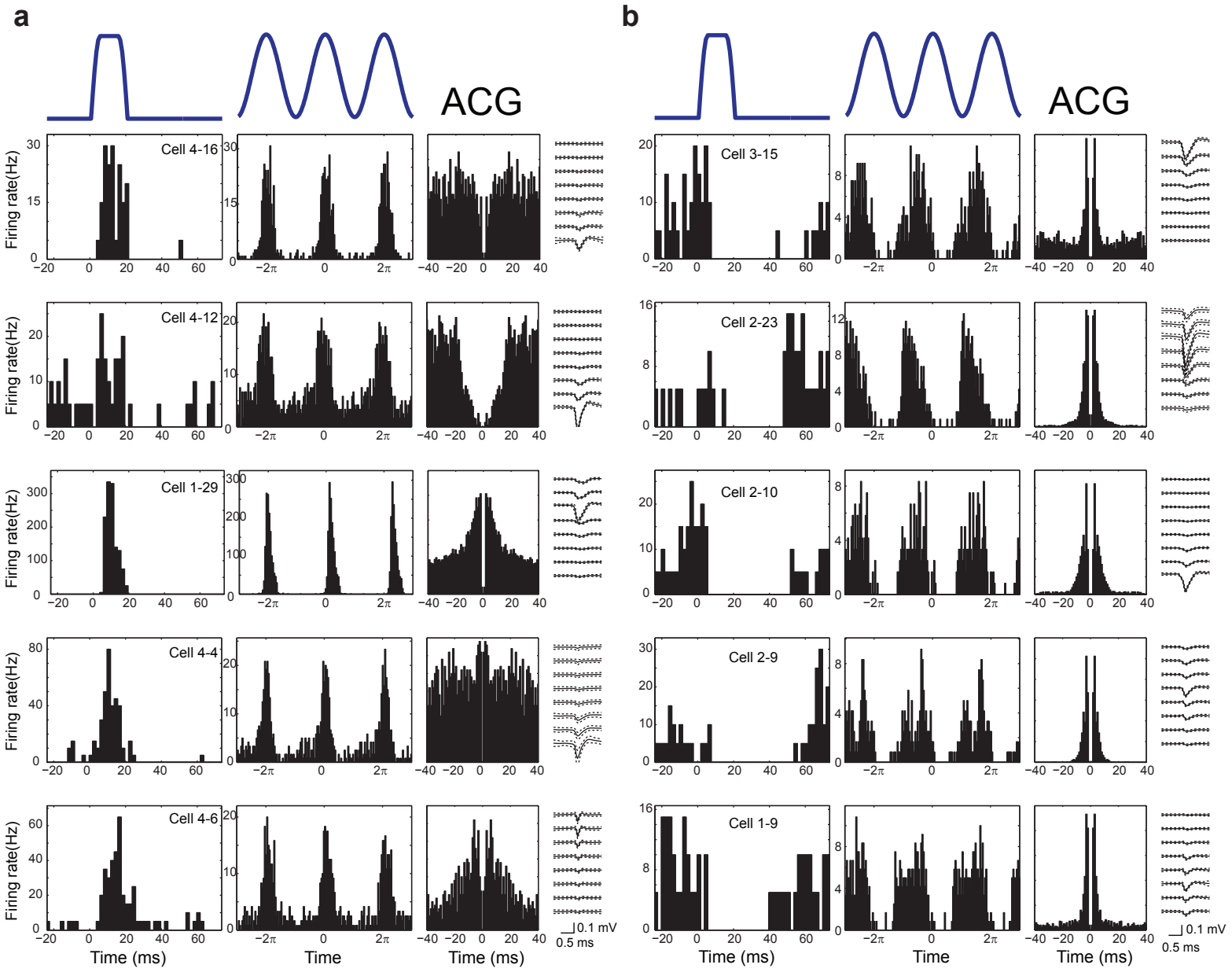

Supplementary Figure 9. Light activation of *Pvalb*+ neurons in the reticular nucleus of the thalamus in the *Pvalb*-IRES-Cre;Ai32 mice (providing additional examples to **Fig. 7c**). (**a**) Each row is an activated reticular neuron. Evoked responses by single pulse (20 ms) or sinus (10 Hz) stimulation, ACG, and mean waveform of the neurons recorded at each of the 8 sites of the silicon probe shank (4-shank probes were used to record simultaneously from both reticular nucleus and neighboring ventrolateral nucleus of thalamus). (**b**) Same arrangement, showing 5 example thalamocortical neurons. Note ACG typical of bursting thalamocortical cells and their difference from the light-activated reticular neurons.